ACS APPLIED MATERIALS & INTERFACES

Research Article

www.acsami.org

Exploitation and Application of a Highly Sensitive Ru(II) Complex-Based Phosphorescent Chemodosimeter for Hg^{2+} in Aqueous Solutions and Living Cells

Jiaxi Ru,[†] Xiaoliang Tang,*[,†,§] Zhenghua Ju,[†] Guolin Zhang,[†] Wei Dou,[†] Xiangquan Mi,[‡] Chunming Wang,[‡] and Weisheng Liu*[,†,§]

[†]Key Laboratory of Nonferrous Metal Chemistry and Resources Utilization of Gansu Province and State Key Laboratory of Applied Organic Chemistry, College of Chemistry and Chemical Engineering and [‡]School of Life Sciences, Lanzhou University, Lanzhou, 730000, China

Supporting Information

ABSTRACT: A novel Ru(II) complex-based phosphorescent probe **Rubpy-1** was designed and synthesized conveniently by incorporating of chemodosimeter into the luminophor, which exhibits good water solubility, longer excitation wavelength, and rapid turn-on phosphorescent response only toward Hg^{2+} in aqueous system under physiological pH. The spectral response mechanism and Hg^{2+}-promoted structure change of the chemodosimeter were analyzed in detail by theoretical calculations and electrospray ionization mass spectrometry. When time-resolved photoluminescence techniques were used, the **Rubpy-1** could eliminate effectively the signal interference from the short-lived background fluorescence in complicated media, accompanied by the significant improvement of the signal-to-noise ratio and the accuracy of the detection. Furthermore, **Rubpy-1** showed low cytotoxicity and excellent membrane permeability toward living cells, which was successfully applied to monitor intracellular Hg^{2+} effectively by confocal luminescence imaging.

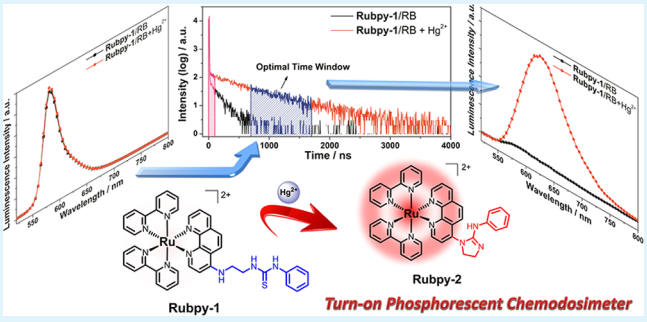

KEYWORDS: *Ru(II) complex, chemodosimeter, phosphorescence, Hg^{2+} recognition, TRES, cell imaging*

1. INTRODUCTION

Functional phosphorescent complexes as versatile materials for applications in chemosensors and bioimaging have gained wide attention during recent years due to their abundant photophysical, photochemical, and electrochemical properties.[1−6] Many transition metal ions, including Pt(II), Re(I), Ir(III), Ru(II), and Au(I) have been used to construct excellent phosphorescent luminophores, which exhibit high luminescence efficiency, significant Stokes shifts, tunable excitation, and emission wavelength over whole visible range, and long lifetimes compared with pure organic luminophores.[7−11] Among these phosphorescence complexes, Ru(II) complexes with polypyridyl ligands are enjoying an increasing interest in the fields of luminescent bioprobes, dye-sensitized solar cells, molecular catalysts, and so on.[12−15] In particular, many Ru(II) complexes have been used as DNA structural probes, which feature unique visible emission change and good biological compatibility.[12,16−19] However, only a few complexes were investigated for detecting bioactive molecules, cation, and anion.[20−25] Moreover, it is worth noting that most chemosensors based on Ru(II) complexes were used only as special luminophores, and the advantage of phosphorescence complexes with long lifetime was rarely presented and applied to improve signal-to-noise ratio of the detection. Therefore, the vast potential of Ru(II) complex as sensor needs to be developed and researched further.

To exploit and develop the great potential of phosphorescence complexes, time-resolved photoluminescent technique (TRPT) is considered to be one of most valuable tools, which can provide the spectral and temporal evolution of the emission of a sample following its illumination by a short pulse of light, and is widely used as luminescence probes, biolabels, and clinical diagnostics.[26−28] By using the method, these long-lifetime luminescent compounds can effectively eliminate the undesirable short-lived autofluorescence and/or scattered light in environmental and biological samples by exerting an appropriate time delay between pulsed excitation and acquisition of signals.[29−33] Some luminescence lanthanide complexes with millisecond lifetimes have been developed as time-resolved photoluminescent probes and exhibited potential applications.[34,35] However, most of them could only be excited by high-energy UV light (<370 nm) and were significantly affected by solvents, which limit their further utilization to some extent.[36−39] Compared with lanthanide complexes, Ru(II)

Received: December 4, 2014
Accepted: February 2, 2015
Published: February 10, 2015

DOI: 10.1021/am508484q
ACS Appl. Mater. Interfaces 2015, 7, 4247−4256

Scheme 1. Synthetic Routes of Chemodosimeter Rubpy-1 and Its Cyclized Product Rubpy-2[a]

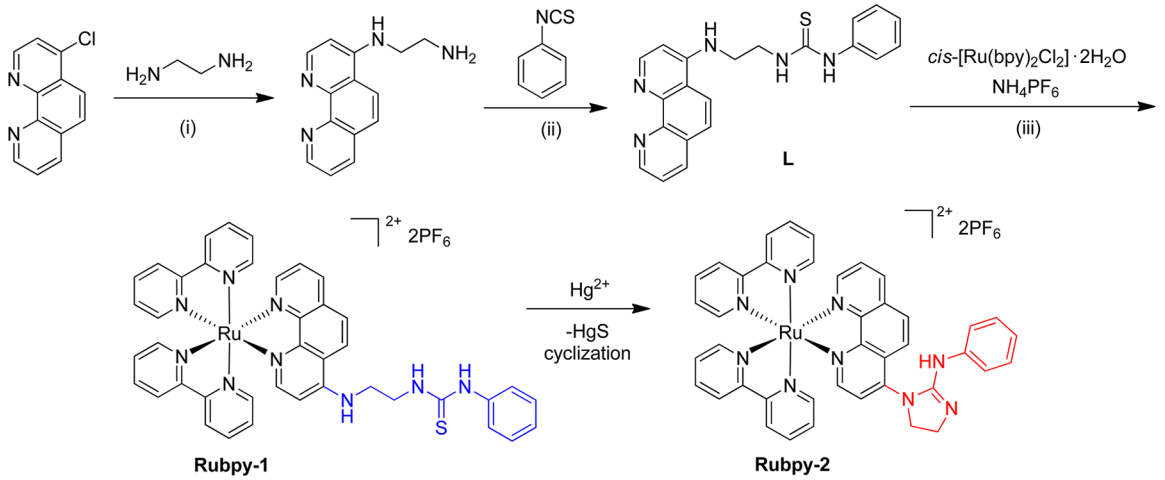

[a]Reagents and conditions: (i) $CHCl_3$, reflux, 6 h; (ii) acetone, 328 K, 5 h; (iii) CH_2Cl_2/ methanol (1:1 v/v), reflux, N_2, 24 h.

polypyridyl complexes not only possess excellent high stability and solubility in water but also have relatively long lifetime in microsecond level and can be excitated by visible light. Hence, Ru(II) complexes are very interesting candidates for TRPT research.

On the other hand, the signal transduction for detecting toxic metal ions is a significant issue in fields as diverse as chemistry, biology, and environmental and material sciences.[40−45] Among the toxic trace metal ions, Hg^{2+} is considered to be one of the most hazardous environmental pollutants, which is widespread and occurs through a variety of natural and anthropogenic sources. Exposure to Hg^{2+} contamination even in quite low concentration also could increase deleterious effects for human beings in the cardiovascular, gastrointestinal, and neurological systems.[46−48] At present, most of the reported Hg^{2+}-selective probes are based on organic fluorescent luminophores, many of which are more or less influenced by some external factors, such as excitation power efficiency, the detector sensitivity, and sample environment (pH, polarity, temperature, redox potential, and so forth).[40−43,49] Thus, it is worth looking forward to the development and application of novel Ru(II) complex-based phosphorescent sensors for recognization of Hg^{2+} in time-resolved photoluminescent analysis and bioimaging studies.

As one of the promising sensing strategies, chemodosimeter has attracted increasing attention because of irreversible chemical reaction between dosimeter molecule and target species, which could cause specific spectral response in the emission or absorption spectra. Thus, this kind of sensor has inherent advantages in accuracy and selectivity of detection compared with those based on coordination effect.[42,43] Taking the above needs into consideration and following our interest in improving detection accuracy and sensitivity of probes, the incorporation of chemodosimeter into phosphorescent Ru(II) complex as a powerful tool should be introduced. Utilizing Hg^{2+}-promoted desulfation and intramolecular cyclic guanylation of thiourea reaction,[50−52] we report herein design and synthesis of a new phosphorescent chemodosimeter, $[Ru(bpy)_2(\mathbf{L})]\cdot(PF_6)_2$ (**Rubpy-1**) (**L** = 1-(2-((1,10-phenanthrolin-4-yl)amino)ethyl)-3-phenylthiourea, bpy = 2,2′-bipyridine, Scheme 1), which exhibits excellent phosphorescence enhancement response only to Hg^{2+} in water or buffer solutions. The mechanism of phosphoresce change has been analyzed in detail by theoretical calculations, and the application of **Rubpy-1** with long emission lifetime in time-resolved luminescence assay has been well-demonstrated. Finally, **Rubpy-1** showed low cytotoxicity and excellent membrane permeability toward living cells, which could be successfully applied to monitor intracellular Hg^{2+} effectively by confocal luminescence imaging.

2. EXPERIMENTAL SECTION

2.1. Materials. All the materials for synthesis were purchased from commercial suppliers and used without further purification. All of the solvents used were of analytical reagent grade, and deionized water was used. All metal salts used were soluble perchlorates or nitrates. (***Caution!*** *Perchlorate salts are potentially explosive. All compounds containing perchlorates should be handled with great care and in small amounts.*) *N*-(2-hydroxyethyl)piperazine-*N*′-ethanesulfonic acid (HEPES) buffer solutions (10 mM, pH = 7.2) were prepared in water. All measurements were carried out in water or HEPES buffer solutions.

2.2. Instruments. ^{1}H NMR and ^{13}C NMR spectra were recorded on JNM-ECS-400 MHz or Varian INOVA 600 spectrometer and referenced to the solvent signals. High-resolution mass spectra (HRMS) were obtained on a Bruker microTOF-Q II mass spectrometer. UV−vis absorption spectra were recorded on Shimadzu UV-2550 spectrophotometer. Phosphorescence spectra were measured using a Hitachi F-7000 spectrophotometer. The lifetimes were determined by FLS920 of Edinburgh Instruments. Luminescence quantum yields at room temperature were measured by the optically dilute method with an aerated aqueous solution of $[Ru(bpy)_3]Cl_2$ (Φ_{em} = 0.028) as the standard solution.[53] All pH measurements were made with a pH-10C digital pH meter.

2.3. Synthesis of L. To a stirred ethylenediamine (50 mL) was added dropwise the solution of 4-chloro-1,10-phenanthroline (2.65 g, 12.0 mmol) in 10 mL of $CHCl_3$ at 0 °C. The reaction mixture was refluxed for 6 h and then cooled to room temperature. The solvent was removed under reduced pressure, and the crude product was added into ice water (30 mL). The pH value was adjusted to 10−12 by using 2 M NaOH solution. The resulting aqueous phase was extracted with $CHCl_3$ (100 mL × 3). Then, the solvent was removed under vacuum to quantitatively obtain red oil product, *N*′-(1,10-phenanthrolin-4-yl)ethane-1,2-diamine, which was used directly without further purification. Then, phenyl isothiocyanate (1.70 g, 12.6 mmol) was added dropwise to the solution of above product in 30 mL of acetone, which was stirred at 328 K for 5 h. After the reaction cooled, precipitates produced in the reaction were filtered, washed with ethanol, and then dried under vacuum. The goal product **L** was

DOI: 10.1021/am508484q
ACS Appl. Mater. Interfaces 2015, 7, 4247−4256

obtained directly as a pale yellow solid. Yield: 3.02 g, 67%. ^{1}H NMR (400 MHz, deuterated dimethyl sulfoxide (DMSO-d_6)): δ 9.85 (s, 1H), 9.00 (dd, J = 4.3, 1.8 Hz, 1H), 8.55 (d, J = 5.5 Hz, 1H), 8.39 (dd, J = 8.2, 1.7 Hz, 1H), 8.19(d, J = 9.2 Hz, 1H), 8.16 (s, 1H), 7.77 (d, J = 9.2 Hz, 1H), 7.69 (dd, J = 8.1, 4.3 Hz, 1H), 7.41 (s, 1H), 7.37 (dd, J = 8.6, 1.7 Hz, 2H), 7.35−7.27 (m, 2H), 7.12 (m, 1H), 6.91 (d, J = 5.5 Hz, 1H), 3.87 (d, J = 5.8 Hz, 2H), 3.55 (d, J = 5.0 Hz, 2H). ^{13}C NMR (100 MHz, DMSO-d_6): δ 180.55, 149.35, 144.97, 141.66, 140.54, 133.22, 130.65, 130.16, 128.76, 124.38, 123.31, 122.13, 121.89, 98.29, 42.73, 42.36. Electrospray ionization mass spectrometry (ESI-MS) m/z: calcd for $C_{21}H_{19}N_5S$ 373.1361 and $[M + H]^+$ 374.1439; found: 374.1443 $[M + H]^+$.

2.4. Synthesis of Rubpy-1. A mixture of *cis*-$[Ru(bpy)_2Cl_2]\cdot 2H_2O$ (187 mg, 0.36 mmol) and **L** (135 mg, 0.36 mmol) in 50 mL of CH_2Cl_2/methanol (1:1 v/v) was refluxed under an inert atmosphere of argon in the dark for 24 h. The mixture was evaporated to dryness, and the solid was dissolved in CH_2Cl_2 and purified by column chromatography on silica gel. The product was eluted with CH_2Cl_2/methanol (4:1 v/v). After the solvent was reduced to ca.5 mL by rotary evaporation, a saturated aqueous solution of NH_4PF_6 was added. The precipitate was filtered affording **Rubpy-1** as an orange solid. Yield: 200 mg (52%). ^{1}H NMR (400 MHz, DMSO-d_6): δ 8.84 (d, J = 8.4 Hz, 2H), 8.81 (d, J = 8.2 Hz, 2H), 8.65 (d, J = 7.6 Hz, 1H), 8.55 (d, J = 9.1 Hz, 1H), 8.42 (s, 1H), 8.25−8.12 (m, 3H), 8.08 (t, J = 7.8 Hz, 2H), 8.03 (d, J = 5.1 Hz, 2H), 7.83 (dd, J = 10.1, 5.3 Hz, 2H), 7.77 (dd, J = 8.2, 5.2 Hz, 1H), 7.67 (d, J = 5.6 Hz, 1H), 7.62 (d, J = 5.1 Hz, 1H), 7.59−7.49 (m, 2H), 7.41−7.34 (m, 2H), 7.32 (d, J = 6.4 Hz, 1H), 7.28 (m, 4H), 7.17−7.08 (m, 1H), 7.05 (d, J = 6.6 Hz, 1H), 3.77 (m, 2H), 3.57 (m, 2H). ^{13}C NMR (150 MHz, DMSO-d_6): δ 180.51, 157.24, 156.84, 156.77, 156.58, 151.71, 151.57, 151.32, 151.18, 151.08, 150.97, 149.97, 147.00, 146.39, 138.61, 137.40, 137.35, 137.22, 136.31, 130.05, 128.77, 127.59, 125.87, 124.78, 124.57, 124.30, 124.20, 123.44, 122.28, 119.69, 104.33, 42.04, 41.82. ESI-MS m/z: calcd for $C_{41}H_{35}N_9SRuP_2F_{12}$ 1077.1063 and $[C_{41}H_{35}N_9SRu]^{2+}$ 393.5890; found: 393.5865 $[M-2PF_6]^{2+}$.

2.5. Synthesis of Rubpy-2. Complex **Rubpy-1** (75 mg, 0.07 mmol) and $Hg(ClO_4)_2\cdot 3H_2O$ (36 mg, 0.08 mmol) were stirred in 20 mL of acetonitrile/H_2O (4:1 v/v) for 2 h at room temperature. The solid formed was removed by filtration. The solution was concentrated by evaporation. The product was purified by silica gel column chromatography with CH_2Cl_2/MeOH (4:1 v/v) to give **Rubpy-2** as an orange solid. Yield: 60 mg (82%). ^{1}H NMR (400 MHz, DMSO-d_6): δ 9.01−8.72 (m, 6H), 8.53 (m, 1H), 8.34 (m, 2H), 8.28−8.02 (m, 6H), 7.98−7.71 (m, 4H), 7.68−7.20 (m, 9H), 6.97 (m, 1H), 4.61−4.14 (m, 2H), 4.14−3.75 (m, 2H). ^{13}C NMR (150 MHz, DMSO-d_6): δ 157.25, 156.84, 156.78, 156.60, 155.79, 151.74, 151.59, 151.31, 151.09, 150.97, 150.11, 148.62, 147.03, 146.86, 146.38, 140.17, 138.04, 137.42, 137.24, 136.34, 130.07, 128.64, 127.98, 127.61, 125.89, 124.85, 124.31, 122.07, 121.03, 119.62, 117.88, 104.18, 54.88, 43.18. ESI-MS m/z: calcd for $C_{41}H_{33}N_9RuP_2F_{12}$ 1043.1186 and $[C_{41}H_{33}N_9Ru]^{2+}$ 376.5951; found: 376.5979 $[M-2PF_6]^{2+}$.

2.6. Theoretical Calculations. The calculation was performed using the Gaussian 09 suite of programs.[54] The ground-state structure of complexes were optimized using density functional theory (DFT) with Becke's three parameter hybrid functional with the Lee−Yang−Parr correlation functional (B3LYP)[55] and 6-31+G(d)/LanL2DZ basis set. The LanL2DZ basis set was used to treat the ruthenium atom,[56] whereas the 6-31+G(d) basis set was used to treat all other atoms.[57] The excited-state related calculations were carried out with the time-dependent density functional theory (TD-DFT) with the optimized structure of the ground state.[58] Seventy singlet absorptions of **Rubpy-1** and **Rubpy-2** were obtained. The polarized continuum model method (CPCM) with water as solvent was used to calculate all the electronic structures in solution.[59] There are no imaginary frequencies in frequency analysis of all calculated structures; therefore, each calculated structure expresses an energy minimum. To understand the nature of the excited state, the orbital analyses of the complexes were also performed,[60] and the contours of the highest occupied molecular orbitals (HOMOs) and lowest unoccupied molecular orbitals (LUMOs) were plotted.

2.7. Time-Resolved Luminescence Detection. Time-resolved emission spectra (TRES) were obtained through a time-correlated single photon counting (TCSPC) technique by using a FLS920 instruments (Edinburgh, U.K.) under excitation of 450 nm. The luminescence signal from 525 to 800 nm was collected and recorded with a R928-P at a step size of 5 nm. Rhodamine B as typical fluorescent interference with short emission lifetime of 1.74 ns was added into the HEPES buffer (10 mM, pH 7.2) solutions containing **Rubpy-1**.[61] Delayed photoluminescence spectra of the mixture of **Rubpy-1** (10 μM) and Rhodamine B (10 μM) acquired after 100 ns can eliminate completely fluorescence of Rhodamine B.

2.8. Cell Culture and Cytotoxicity Tests. SMMC-7721 cells were maintained in RPMI-1640 medium supplemented with 10% heat-inactivated fetal calf serum, 100 units per milliliter of penicillin, and 100 μg mL^{-1} streptomycin at 37 °C under humidified atmosphere containing 5% CO_2. Cells (5×10^8 L^{-1}) were plated on 18 mm glass coverslips, allowed to adhere for 24 h, treated with **Rubpy-1** (20 μM), and then incubated for 30 min. Subsequently, the cells were treated with 100 μM $Hg(ClO_4)_2$. Cells were incubated for 30 min and rinsed with phosphate-buffered saline (PBS) three times to remove free compound and ions before analysis. SMMC-7721 cells only incubated with 20 μM **Rubpy-1** for 30 min acted as a control. Confocal luminescence images of SMMC-7721 cells were carried out on an Olympus FV1000 laser scanning confocal microscope with a 100× oil-immersion objective lens. The cytotoxic activity experiment of complex against SMMC-7721 cells was tested according to standard 3-(4,5-dimethylthiazole)-2,5-diphenyltetraazolium bromide (MTT) assay procedures.[62]

3. RESULTS AND DISCUSSION

3.1. Phosphorescent Response toward Hg^{2+}. The absorption and luminescence spectra of **Rubpy-1** in the absence and presence of Hg^{2+} are shown in Figure S1 (Supporting Information), and the corresponding data are listed in Table 1. At ambient temperature, chemodosimeter

Table 1. Photophysical Properties of Rubpy-1 in the Absence and Presence of Hg^{2+} in HEPES Buffer (10 mM, pH 7.2) Solutions

compound	$\varepsilon_{450\ nm}$ (M^{-1} cm^{-1})	λ_{em} (nm)	Φ_p[a] (%)	brightness[b] (M^{-1} cm^{-1})	τ[c] (ns)
Rubpy-1	7600	616	0.4	30.4	215
Rubpy-1+Hg^{2+}	8700	611	2.2	191.4	785

[a]Relative phosphorescence quantum yield with respect to $[Ru(bpy)_3]Cl_2$ (Φ = 0.028 in air-equilibrated water) standard. [b]Brightness = $\varepsilon_{450\ nm} \times \Phi_p$. [c]$\tau = \sum A_i\tau_i^2/\sum A_i\tau_i$ (i = 1−2).

Rubpy-1 (10 μM) exhibited a weak and broad emission band centered at 616 nm with luminescence quantum yield ca. 0.004 in HEPES buffer (10 mM, pH 7.2) solutions. The UV−vis absorption spectrum of **Rubpy-1** displayed intense absorption bands in the ultraviolet region of 260−360 nm with extinction coefficients (ε) of ~4 × 10^4 L·mol^{-1}·cm^{-1}, which could be assigned to spin-allowed intraligand ($\pi \rightarrow \pi^*$) transitions of 2,2′-bipyridine (bpy) ligands and 1,10-phenanthroline ligand. Meanwhile, there was a low-energy broad absorption band at 360−560 nm with extinction coefficients (ε) of ~1 × 10^4 L·mol^{-1}·cm^{-1}, predominantly attributed to an overlap of the spin-allowed metal-to-ligand charge-transfer transition (^{1}MLCT, $d\pi$(Ru) → π^*(bpy and **L**)), ligand-to-ligand charge-transfer transition (^{1}LLCT, π(**L**) → π^*(bpy)), and intraligand charge-transfer transition (^{1}ILCT, π(**L**) → π^*(**L**)), as confirmed by TD-DFT calculations (vide infra).

DOI: 10.1021/am508484q
ACS Appl. Mater. Interfaces 2015, 7, 4247−4256

Upon the addition of Hg^{2+} ions, the low-energy absorption bands of **Rubpy-1** centered at 450 nm and high-energy absorption bands centered at 270, 284, and 310 nm increased progressively with a concomitant decrease of absorption from 330 to 410 nm (Figure 1). Two well-defined isosbestic points

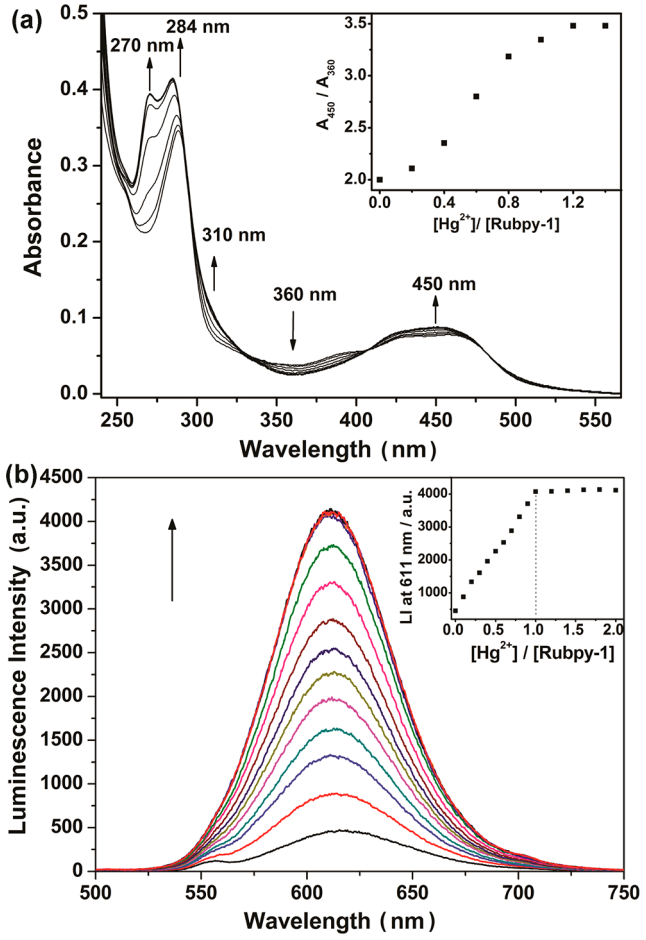

Figure 1. (a) UV−vis absorption changes and (b) luminescence spectral changes of **Rubpy-1** upon addition of Hg^{2+} in HEPES buffer (10 mM, pH 7.2) solutions at room temperature. (a, inset): Absorbance changes of $A_{450\ nm}/A_{360\ nm}$ as a function of the concentration rate of $[Hg^{2+}]/[$**Rubpy-1**$]$. (b, inset): Luminescence changes vs the concentration rate of $[Hg^{2+}]/[$**Rubpy-1**$]$ at 611 nm. [**Rubpy-1**] = 10 μM, λ_{ex} = 467 nm.

occur at 331 and 408 nm, indicating that a new species is produced. The variation of absorption intensity ratio at 450 and 360 nm ($A_{450\ nm}/A_{360\ nm}$) increased continuously until equal amounts of Hg^{2+} were used. When more Hg^{2+} was added, the absorption stopped growing further, which showed 1:1 stoichiometry between metal ion and **Rubpy-1** (Figure 1a, inset). Also, the luminescence intensity of **Rubpy-1** at maximum emission increased linearly with the amount of Hg^{2+} in the range of 0−10 μM, consistent with the stoichiometry obtained from the UV−vis absorption spectra. About 9-fold enhancement with slight blue-shift was observed finally, and the quantum yield achieved 0.022, which showed a turn-on phosphorescent response toward Hg^{2+} and larger Stokes shift (~150 nm) (Figure 1b). In addition, the phosphorescent responses of **Rubpy-1** for Hg^{2+} were similar in water, HEPES, and PBS buffer solutions, which showed wider applicability in different solution systems (Figure S2, Supporting Information). From the linear equation of spectra titration at 611 nm, the detection limit of **Rubpy-1** for Hg^{2+} was calculated to be 8 nM (1.6 ppb) at the signal-to-noise ratio (S/N) = 3 (Figure S3, Supporting Information), below the limited level of Hg^{2+} ion in drinking water regulated by the U.S. Environmental Protection Agency (2.0 ppb).[63] Furthermore, the spectral response could not be found for other metal ions.

The optical sensing properties of chemodosimeter are mainly dominated the specificity of chemical reaction between dosimeter molecule and target species. The selectivity of **Rubpy-1** toward common metal ions, including Li^{+}, Na^{+}, K^{+}, Mg^{2+}, Ca^{2+}, Al^{3+}, Fe^{3+}, Co^{2+}, Ni^{2+}, Cu^{2+}, Cr^{3+}, Pb^{2+}, Cd^{2+}, Ag^{+}, Mn^{2+}, Zn^{2+}, and Hg^{2+}, was systematically investigated in HEPES buffer (10 mM, pH 7.2, 50 mM NaCl) solutions. Variations of luminescence spectra of **Rubpy-1** (10 μM) were recorded within 5 min after the addition of 10 equiv of various metal ions. As shown in Figure 2a, significant enhancement of luminescence intensity at 611 nm was observed only for Hg^{2+}, while the addition of other metal ions could not cause any obvious luminescent change. Moreover, the cation-competitive experiments were done to deeply examine the selectivity and anti-interference of **Rubpy-1**. As shown in Figure 2b, it clearly showed that the luminescence emission of **Rubpy-1** in the

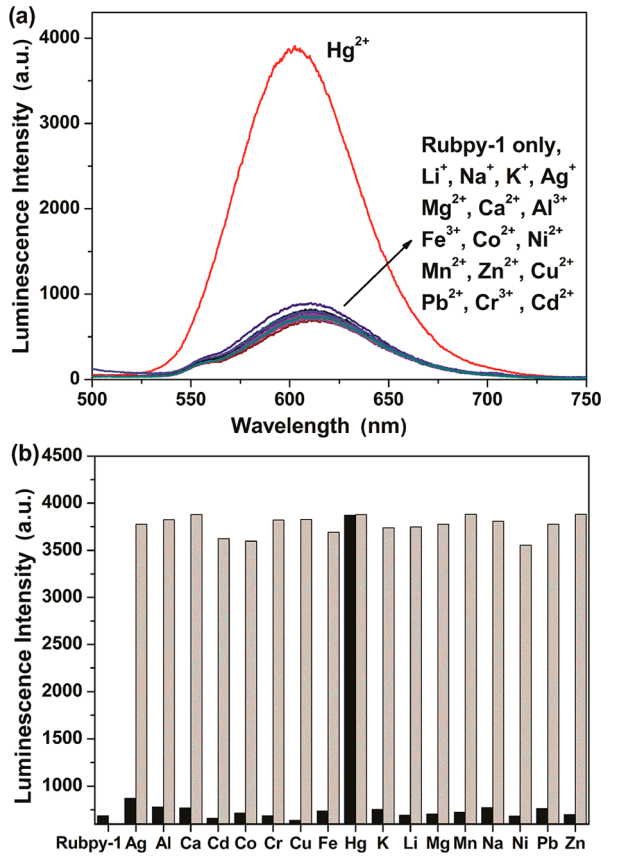

Figure 2. (a) Luminescence spectra of **Rubpy-1** upon the addition of various metal ions (Li^{+}, Na^{+}, K^{+}, Mg^{2+}, Ca^{2+}, Al^{3+}, Fe^{3+}, Co^{2+}, Ni^{2+}, Cu^{2+}, Cr^{3+}, Pb^{2+}, Cd^{2+}, Ag^{+}, Mn^{2+}, Zn^{2+}, and Hg^{2+}) within 5 min in HEPES buffer (10 mM, pH 7.2, 50 mM NaCl) solutions. (b) Relative luminescence intensities of **Rubpy-1** at 611 nm in HEPES buffer solutions. Black bars represent addition of various metal ions to the solution of **Rubpy-1**. Gray bars represent addition of Hg^{2+} and various metal ions to the solution of **Rubpy-1**. [**Rubpy-1**] = 10 μM, $[M^{n+}]$ = 100 μM, λ_{ex} = 467 nm.

DOI: 10.1021/am508484q
ACS Appl. Mater. Interfaces 2015, 7, 4247−4256

presence of Hg^{2+} was still outstanding, and the selective sensing behavior for Hg^{2+} was hardly interfered by commonly coexistent metal ions. Furthermore, the selectivity of **Rubpy-1** to common anions was also investigated in HEPES buffer (10 mM, pH 7.2) solutions (Figure S4, Supporting Information). The results exhibited that there was no obvious change in luminescence intensity in the presence of various anions, including F^-, Cl^-, Br^-, I^-, NO_2^-, NO_3^-, HSO_3^-, SO_4^{2-}, S^{2-}, PO_4^{3-}, $P_2O_7^{4-}$, and CH_3COO^- (as their sodium salts), which further confirmed that **Rubpy-1** possessed high selectivity toward Hg^{2+} and was hardly affected by common anions. In addition, as chemodosimeter, there was also no obvious change for the emission of **Rubpy-1** when the excess amount of $EDTA^{2-}$ was added into **Rubpy-1** or the mixture of **Rubpy-1** and Hg^{2+} in HEPES buffer solution, indicating that **Rubpy-1** reacts with Hg^{2+} irreversibly (Figure S5, Supporting Information). Thus, **Rubpy-1** showed excellent selectivity and accuracy for Hg^{2+} through phosphorescent enhancement response in aqueous media and complex environment.

For chemodosimeter, signal response time depends on the rate of reaction between dosimeter molecule and target species. Thus, the reaction kinetics for the time-dependent dosimetric response was evaluated between **Rubpy-1** and Hg^{2+}. As shown in Figure 3, the luminescence of **Rubpy-1** always remained

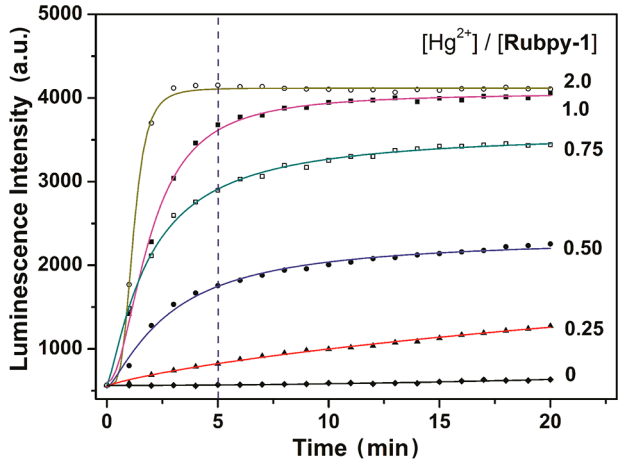

Figure 3. Luminescence response changes of **Rubpy-1** at 611 nm over time with the addition of (0, 0.25, 0.50, 0.75, 1.0, 2.0 equiv) Hg^{2+} ions in HEPES buffer (10 mM, pH 7.2) solutions. [**Rubpy-1**] = 10 μM, λ_{ex} = 467 nm.

untouched in the absence of Hg^{2+} over time, but the time needed for emission intensity of **Rubpy-1** (10 μM) to gradually reach stable state at 611 nm was obviously shortened with the increasing of the ratio of [Hg^{2+}]/[**Rubpy-1**] in HEPES buffer (10 mM, pH 7.2) solutions. When concentration ratio of [Hg^{2+}]/[**Rubpy-1**] is more than 1, the progress curve of the kinetic analysis clearly demonstrated that the emission intensity of **Rubpy-1** quickly increased in the first 2 min and reached relative maximum within 5 min. The other metal ions, for example, thiophilic Ag^+ or Cu^{2+}, could not cause the obvious change of the luminescence emission of **Rubpy-1** even at higher concentration as time went on (Figure S6, Supporting Information), which makes **Rubpy-1** a practical tool for rapid Hg^{2+} detection.

In addition, the luminescence intensity changes of chemodosimeter **Rubpy-1** as a function of pH in the presence and absence of Hg^{2+} system were also investigated (Figure S7, Supporting Information). For **Rubpy-1**, it showed no dramatic spectral change in wide pH range of 1−9 and enhanced the luminescence emission at higher pH. In the presence of Hg^{2+}, the chemodosimeter **Rubpy-1** exhibited a failing response at lower pH due to the protonation of 1,10-phenanthroline, but it was highly sensitive and stable for metal ion within the pH range of 4−10, within which most biological samples (5.25−8.93) can be tested. As a result, **Rubpy-1** could be applied in living cells without interference from pH effects.

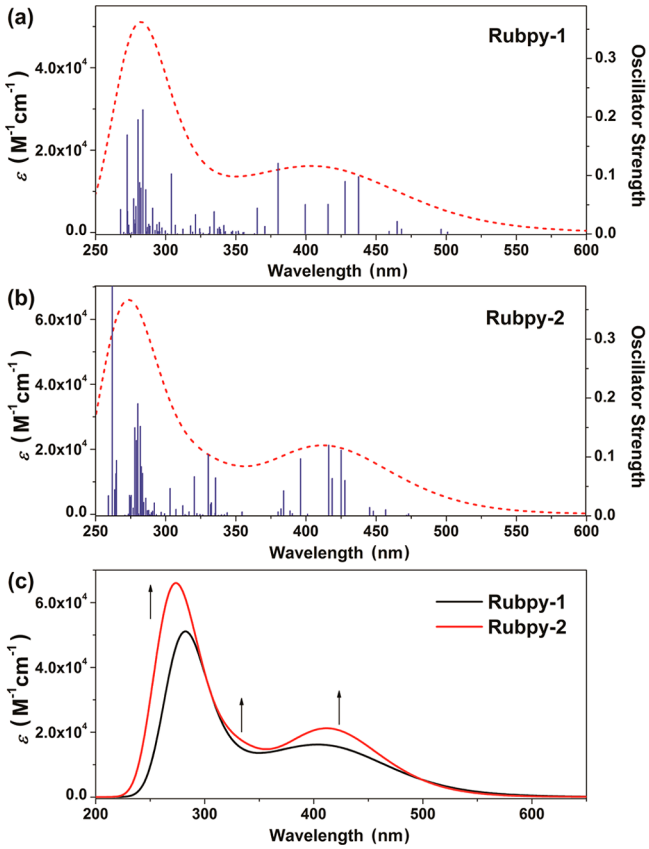

Figure 4. Theoretical UV−vis absorption spectra of **Rubpy-1** (a) and **Rubpy-2** (b). Blue vertical lines correspond to calculated electronic transisitons whereby the height refers to the oscillator strength of the respective transition. The first 70 singlet transitions were calculated. (c) The comparison of calculated UV−vis absorption spectra between **Rubpy-1** and **Rubpy-2**.

3.2. Sensing Mechanism of Chemodosimeter. To gain insight into the sensing mechanism, ESI mass spectral changes of **Rubpy-1** in the absence and presence of Hg^{2+} ions were employed to provide direct evidence of the chemical reaction between chemodosimeter and Hg^{2+}. The **Rubpy-1** displayed a characteristic peak of [**Rubpy-1**−2PF_6]$^{2+}$ at m/z 393.5865. However, after the addition of an excess amount of Hg^{2+} ions, the peak totally disappeared, and a new peak at m/z 376.5979 was found at the same time, which can be assigned to the desulfurized and cyclized product [**Rubpy-2**−2PF_6]$^{2+}$ (Figures S8−S19, Supporting Information). The ^{1}H NMR titration study of **Rubpy-1** showed that two $-CH_2-$ at $\delta \approx 3.75$ ppm moved to upfield and were split with the addition of Hg^{2+}, although there is significant overlap in the aromatic region of the ^{1}H NMR spectra (Figure S20, Supporting Information). In addition, Job's plot analysis of the emission for the mixed solution of **Rubpy-1** and Hg^{2+} exhibited a maximum at ~0.5 mole fraction, assuming 1:1 stoichiometry between the

DOI: 10.1021/am508484q
ACS Appl. Mater. Interfaces 2015, 7, 4247−4256

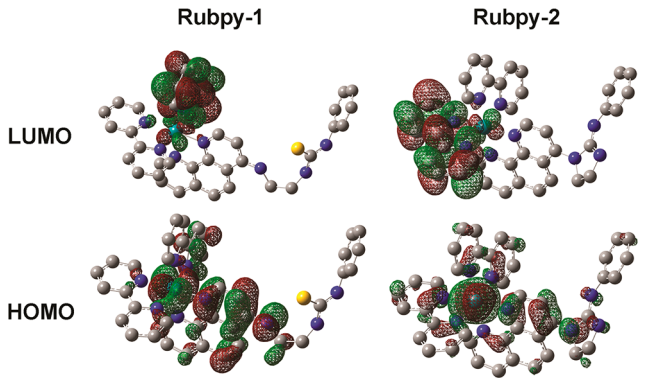

Figure 5. HOMO and LUMO distributions of complexes **Rubpy-1** and **Rubpy-2** based on their optimized geometry structure of triplet state. Hydrogen atoms are omitted for clarity.

chemodosimeter and metal ion (Figure S21, Supporting Information). These results also indicated that the flexible ligand was changed and that five-membered ring structure was formed in the presence of Hg^{2+} ions.

For better understanding the photophysical property and optical response mechanism further, TD-DFT calculations were performed to estimate the corresponding transition energies of **Rubpy-1** and **Rubpy-2**. The ground-state geometries of two complexes were first optimized by DFT calculation (Figure S22 and Tables S1 and S2, Supporting Information). And then, their UV−vis absorption spectra were calculated with TD-DFT based on respective ground-state geometries. As shown in Figure 4a,b, calculated spectral curves of **Rubpy-1** and **Rubpy-2** look broadly similar in whole absorption wavelength range, and singlet transitions reveal that the excitations of both complexes are mainly assigned to an overlap of ^{1}LLCT/^{1}MLCT/^{1}ILCT in the visible region (Table S3−S8, Supporting Information), supported by UV−vis spectral profiles at ∼360−560 nm. However, the energy levels and strengths of the stronger electronic transisitons of **Rubpy-2** are sometimes different from those of **Rubpy-1** according to theoretical calculations, which show a similar trend in good agreement with the experimental absorption changes both in the visible region and in the ultraviolet region (Figure 4c).

On the basis of the optimized geometry structures of triplet state, the lowest-lying triplet transitions of **Rubpy-1** and **Rubpy-2** corresponding to their respective phosphorescence emissions in the visible region also were analyzed and compared. The distributions of the molecular orbitals and the calculated data are showed in Figure 5 and Tables S9−S14 (Supporting Information). For **Rubpy-1**, the contribution to the lowest-lying triplet−triplet transition mainly originates from HOMO → LUMO (91.6%), in which HOMO is mainly localized on the Ru(II) center (47.16%) and 1,10-phenanthroline (30.67%), while LUMO is primarily localized on two bpy

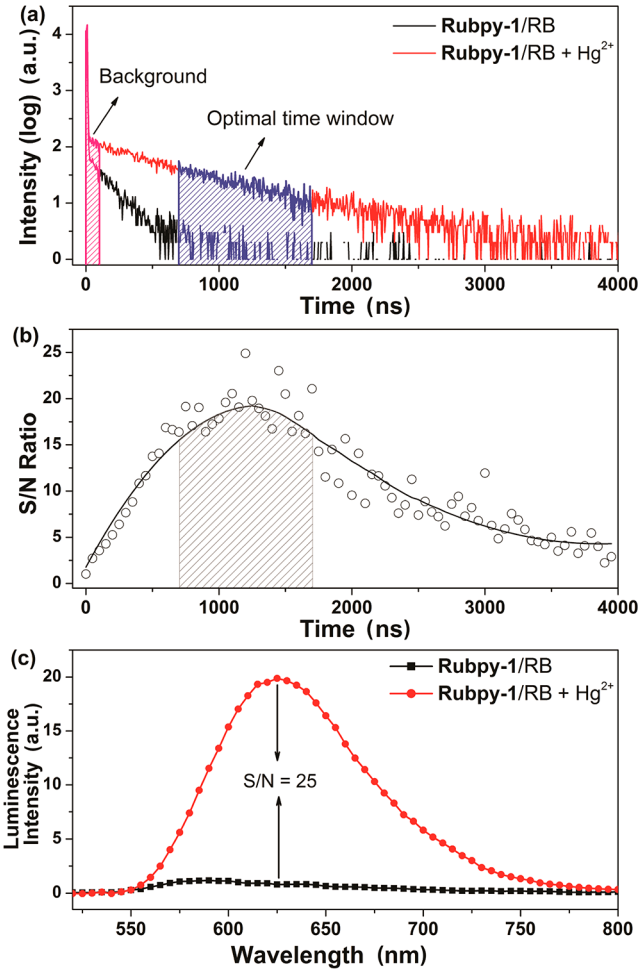

Figure 7. (a) Phosphorescence decay curves of the mixture of **Rubpy-1** and RB in the absence and presence of Hg^{2+} at 625 nm. (b) The change trend of the intensity ratio of two decay curves over time. (c) Photoluminescence spectra of **Rubpy-1** with optimal S/N ratio for detecting Hg^{2+} acquired after 1200 ns delay. [**Rubpy-1**] = [RB] = 10 μM.

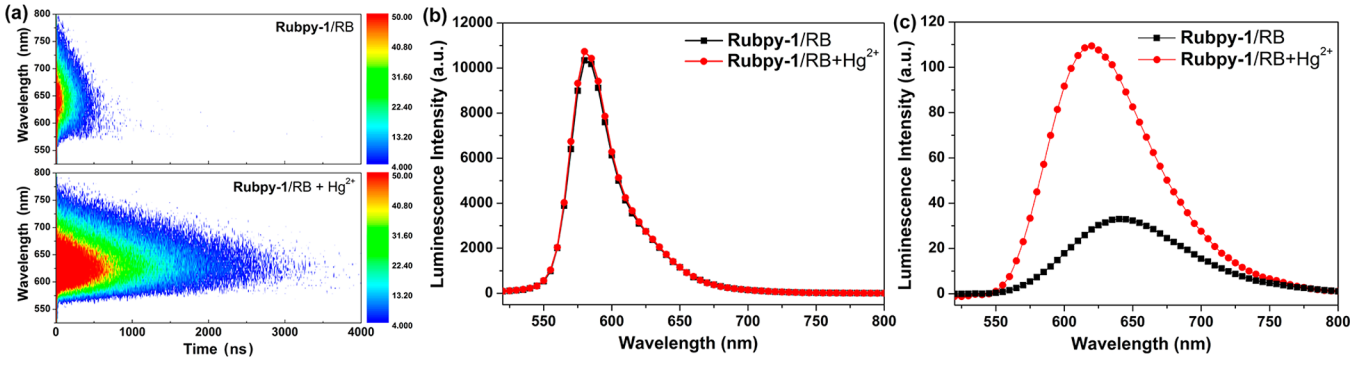

Figure 6. (a) Time-resolved emission spectra of the mixture of **Rubpy-1** and Rhodamine B (RB) in the absence and presence of 5 equiv of Hg^{2+}. Photoluminescence spectra of the mixture acquired after 0 ns delay (b) and 100 ns delay (c). [**Rubpy-1**] = [RB] = 10 μM.

DOI: 10.1021/am508484q
ACS Appl. Mater. Interfaces 2015, 7, 4247−4256

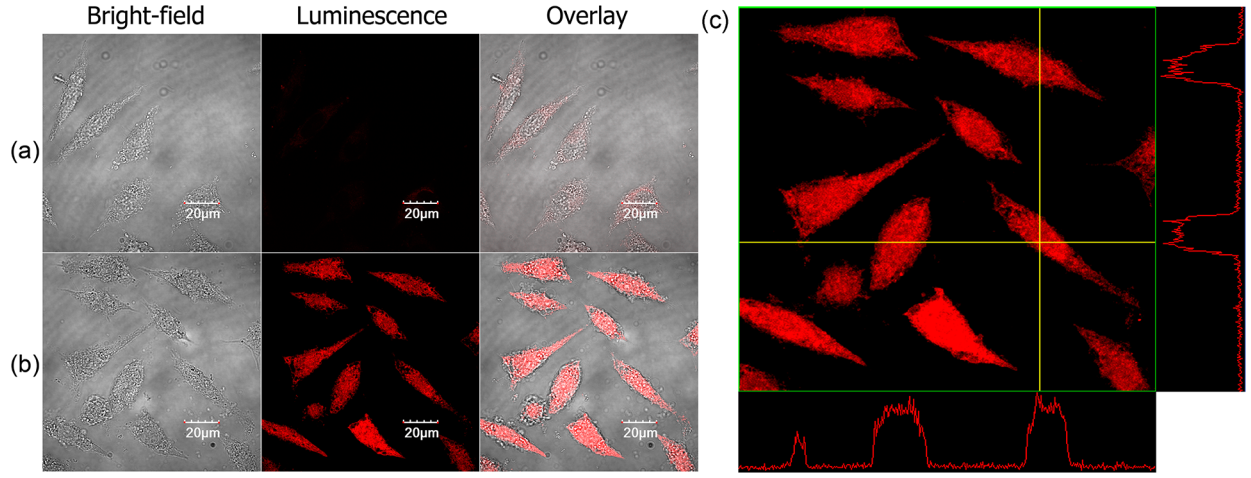

Figure 8. Confocal luminescence images of SMMC-7721 cells. (a) SMMC-7721 cells were incubated with **Rubpy-1** (20 μM) for 30 min at 37 °C. (b) SMMC-7721 cells were incubated with **Rubpy-1** (20 μM) for 30 min and then further incubated with Hg^{2+} (100 μM) for 30 min. (c) Luminescence intensity profile (across the lines) of cells incubated with **Rubpy-1** and Hg^{2+}.

ligands (91.89%). Thus, the phosphorescence emission of **Rubpy-1** could be assigned to an overlap of ^{3}MLCT (π^*(bpy) → dπ(Ru)) and ^{3}LLCT (π^*(bpy) → π(**L**)) that is weak emission. For cyclized product **Rubpy-2**, the contribution to the lowest-lying triplet−triplet transition still comes mainly from HOMO → LUMO (78.5%), and the distribution of LUMO is similar to that of **Rubpy-1** (92.54%). However, the distribution of HOMO is mainly on the Ru(II) center (70.88%), significantly different from that of **Rubpy-1**, which may help to more efficiently increase the transition probability of excited electrons through ^{3}MLCT (π^*(bpy) → dπ(Ru)) and result in the phosphorescent enhancement of **Rubpy-2**. In addition, despite the discrepancy between the calculated emission wavelength and the experimental result, the TD-DFT calculations clearly predicted the trend of blue shift of **Rubpy-2** in phosphorescent emission compared with that of **Rubpy-1**, consistent with slight changes of luminescence spectra.

3.3. Application in Time-Resolved Luminescence Assay. Because of long enough phosphorescence lifetime of Ru(II) complex, **Rubpy-1** could exhibit promising application in time-resolved luminescence detection, which can remove effectively the interference from undesirable scattered light and/or shorter-lived background fluorescence. To demonstrate the merits of phosphorescent chemodosimeter, the TRES experiments of **Rubpy-1** before and after addition of Hg^{2+} were carried out in HEPES buffer (10 mM, pH 7.2) solutions containing Rhodamine B as a typical background interference, which is a common fluorescent dye with short emission lifetime of 1.74 ns, and its emission band completely overlaps with the phosphorescence emission of Ru(II) complexes in the steady-state photoluminescence spectra.

As shown in Figure 6a, under the excitation at 450 nm, TRES experiments visually showed that phosphorescent lifetime of **Rubpy-1** underwent a relative quick decay process in the absence of Hg^{2+} over the range of emission wavelengths, but slow decay when Hg^{2+} was added. Such difference is caused by the formation of cyclized product **Rubpy-2** with different photophysical property. When emission spectra of the mixture of **Rubpy-1** and Rhodamine B were recorded without decay, the maximum emission at 583 nm was dominated by the strong emission of Rhodamine B, and the phosphorescence emission of **Rubpy-1** could not be distinguished and identified, whether or not Hg^{2+} ions were added (Figure 6b). However, TRES of **Rubpy-1** after 100 ns delay completely and effectively removed the Rhodamine B fluorescence contribution, only affording turn-on phosphorescent change of **Rubpy-1** after addition of Hg^{2+} (Figure 6c). Thus, these results successfully highlight the advantage of long-lifetime phosphorescent signal in eliminating the interference from short-lived background fluorescence.

In addition, more meaningfully, the S/N ratio of **Rubpy-1** for detecting Hg^{2+} ions could be further improved by finding optimal time window. As shown in Figure 7a, the attenuation rate of **Rubpy-1** in the presence of Hg^{2+} is much slower than that in the absence of Hg^{2+} at 625 nm, which led to increasing the difference between two attenuation curves. Thus, the changes of the intensity ratio on two curves over time could be used as an index to appraise the S/N ratio of the detection for analyte. Figure 7b obviously exhibits that time-dependent intensity ratio with the maximum difference corresponding to optimal time window appears in the range from 0.7 to 1.7 μs, during which Ru(II) complex not only remains phosphorescent signal to avoid fluorescent interference but also improves the S/N ratio of the detection of Hg^{2+}. When time-resolved acquisition of the spectrum was delayed until 1.2 μs, the optimal S/N ratio of **Rubpy-1** for detecting Hg^{2+} achieved 25 (Figure 7c), much better than that of steady-state spectroscopy methods.

3.4. Application in Intracellular Hg^{2+} Imaging. Considering excellent sensing performance of chemodosimeter **Rubpy-1** to Hg^{2+} in aqueous solutions, the ability of **Rubpy-1** to detect Hg^{2+} within living cells was further tested by confocal luminescence imaging. As shown in Figure 8a, the human hepatoma cells (SMMC-7721) incubated with **Rubpy-1** (20 μM) alone for 30 min at 37 °C kept good shape and appeared viable, which exhibited very weak and red emission from the cytoplasm through comparing with bright-field images of cells. However, the cells treated with **Rubpy-1** were further incubated with Hg^{2+} (100 μM) for another 30 min at 37 °C; all cells displayed remarkable red luminescence, much stronger than luminescence of **Rubpy-1**-stained cells (Figure 8b). In addition, by collecting a series of images of SMMC-7721 cells at different layers from the bottom of the cells in accordance with the *Z*-axis step to the top of cells in Figure S23 (Supporting

DOI: 10.1021/am508484q
ACS Appl. Mater. Interfaces 2015, 7, 4247−4256

Information), the luminescence signals were localized in the whole cell, not only in the cytoplasm, which was further confirmed by the overlap Z-scan confocal image and quantization analysis of luminescence intensity (Figure 8c, Figure S24, Supporting Information). Moreover, to determine the location of organelle in living cells, 4',6-diamidino-2-phenylindole (DAPI) costained experiments were performed to identify nucleus. As shown in Figure S25 (Supporting Information), nucleus showed blue fluorescence whether in the absence or presence of Hg^{2+} after further costained with DAPI for 30 min, which is easily discriminated from the cytoplasm by different colors. Therefore, these results demonstrated that **Rubpy-1** had good cell membrane permeability and good counterstain compatibility with the DNA staining dye DAPI to detect the Hg^{2+} in the entire cell through the luminescence enhancement.

Furthermore, the cytotoxicity of **Rubpy-1** toward SMMC-7721 cells was measured using an MTT assay. As shown in Figure 9, chemodosimeter **Rubpy-1** with water solubility had

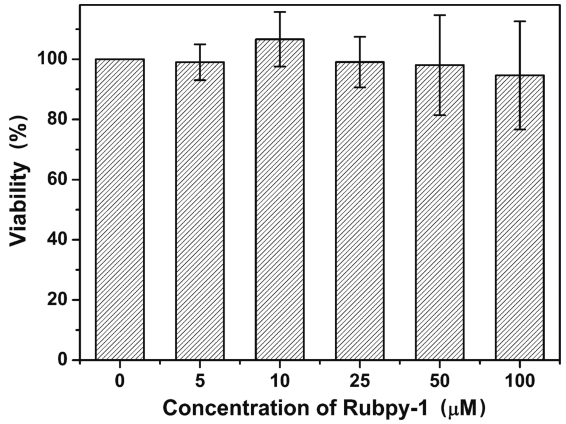

Figure 9. SMMC-7721 cell viability values estimated by MTT proliferation test vs incubation concentrations of **Rubpy-1**. Cells were cultured in the presence of 0–100 μM complex at 37 °C for 24 h.

no significant cytotoxicity to cells. Even though the concentration of complex **Rubpy-1** was as high as 100 μM, the cell viability still remained above 95% after incubation with **Rubpy-1** for 24 h. Therefore, the new phosphorescent chemodosimeter could be an excellent platform and have a great potentiality to apply for detecting and studying the uptake, bioaccumulation, and bioavailability of Hg^{2+} in living cells or organisms.

4. CONCLUSION

In conclusion, we have employed chemodosimeter approach to design and develop a new phosphorescent probe **Rubpy-1** based on Ru(II) complex. The chemodosimeter exhibited good water solubility, longer excitation wavelength, and turn-on phosphorescent response only toward Hg^{2+} in aqueous system, which utilizes irreversible Hg^{2+}-promoted desulfurization and cyclization reaction of the thiourea unit. Despite working as a reaction probe, **Rubpy-1** not only showed phosphorescent response quickly enough, but also had high sensitivity (less than 2.0 ppb) and stability within the pH range of 4–10. When a time-resolved photoluminescence technique was used, phosphorescent **Rubpy-1** could eliminate effectively the signal interference from the short-lived fluorescent background in complicated media, accompanied by significant improvement of the signal-to-noise ratio and the accuracy of the detection for Hg^{2+}. Furthermore, **Rubpy-1** with low cytotoxicity has been successfully used for bioimaging by using confocal laser scanning microscope, which may be favorable for biological applications to monitor and research effectively the bioaccumulation and bioavailability of Hg^{2+} in living cells.

■ ASSOCIATED CONTENT

Ⓢ Supporting Information

The UV–vis absorption and emission spectra, additional spectroscopic material, the detection limit measurement, pH effect, HRMS, ^{1}H NMR, ^{13}C NMR, and IR spectra of the compounds, Job's plot experiment, DFT calculations, calculated molecular structures, confocal images of cells. This material is available free of charge via the Internet at http://pubs.acs.org.

■ AUTHOR INFORMATION

Corresponding Authors

*E-mail: tangxiaol@lzu.edu.cn (X. Tang).
*E-mail: liuws@lzu.edu.cn (W. Liu).

Author Contributions

§These authors contributed equally to this work.

Notes

The authors declare no competing financial interest.

■ ACKNOWLEDGMENTS

This work was supported by NSFC (Grant Nos. 91122007, 21371083, 21001059, 21431002), the Fundamental Research Funds for the Central Universities (lzujbky-2014-192), and the Specialized Research Fund for the Doctoral Program of Higher Education (Grant No. 20110211130002).

■ REFERENCES

(1) Marin, V.; Holder, E.; Hoogenboom, R.; Schubert, U. S. Functional Ruthenium(II)- and Iridium(III)-Containing Polymers for Potential Electro-Optical Applications. *Chem. Soc. Rev.* **2007**, *36*, 618–635.

(2) Zhao, Q.; Huang, C.; Li, F. Phosphorescent Heavy-Metal Complexes for Bioimaging. *Chem. Soc. Rev.* **2011**, *40*, 2508–2524.

(3) You, Y. Phosphorescence Bioimaging Using Cyclometalated Ir(III) Complexes. *Curr. Opin. Chem. Biol.* **2013**, *17*, 699–707.

(4) Lo, K. K.; Li, S. P. Utilization of the Photophysical and Photochemical Properties of Phosphorescent Transition Metal Complexes in the Development of Photofunctional Cellular Sensors, Imaging Reagents, and Cytotoxic Agents. *RSC Adv.* **2014**, *4*, 10560–10585.

(5) Sun, H.; Liu, S.; Lin, W.; Zhang, K. Y.; Lv, W.; Huang, X.; Huo, F.; Yang, H.; Jenkins, G.; Zhao, Q.; Huang, W. Smart Responsive Phosphorescent Materials for Data Recording and Security Protection. *Nat. Commun.* **2014**, *5*, 3601.

(6) Zhang, K. Y.; Zhang, J.; Liu, Y.; Liu, S.; Zhang, P.; Zhao, Q.; Tang, Y.; Huang, W. Core–Shell Structured Phosphorescent Nanoparticles for Detection of Exogenous and Endogenous Hypochlorite in Live Cells via Ratiometric Imaging and Photoluminescence Lifetime Imaging Microscopy. *Chem. Sci.* **2015**, *6*, 301–307.

(7) Yam, V. W.; Cheng, E. C. Highlights on the Recent Advances in Gold Chemistry-a Photophysical Perspective. *Chem. Soc. Rev.* **2008**, *37*, 1806–1813.

(8) Ji, S. M.; Wu, W. H.; Wu, W. T.; Guo, H. M.; Zhao, J. Z. Ruthenium(II) Polyimine Complexes with a Long-Lived ^{3}IL Excited State or a ^{3}MLCT/^{3}IL Equilibrium: Efficient Triplet Sensitizers for Low-Power Upconversion. *Angew. Chem., Int. Ed.* **2011**, *50*, 1626–1629.

(9) Ma, Y.; Liu, S.; Yang, H.; Wu, Y.; Sun, H.; Wang, J.; Zhao, Q.; Li, F.; Huang, W. A Water-Soluble Phosphorescent Polymer for Time-

DOI: 10.1021/am508484q
ACS Appl. Mater. Interfaces 2015, 7, 4247–4256

Resolved Assay and Bioimaging of Cysteine/Homocysteine. *J. Mater. Chem. B* **2013**, *1*, 319−329.
(10) Ma, Y.; Liu, S.; Yang, H.; Wu, Y.; Yang, C.; Liu, X.; Zhao, Q.; Wu, H.; Liang, J.; Li, F.; Huang, W. Water-Soluble Phosphorescent Iridium(III) Complexes as Multicolor Probes for Imaging of Homocysteine and Cysteine in Living Cells. *J. Mater. Chem.* **2011**, *21*, 18974−18982.
(11) Louie, M.; Choi, A. W.; Liu, H.; Chan, B. T.; Lo, K. K. Synthesis, Emission Characteristics, Cellular Studies, and Bioconjugation Properties of Luminescent Rhenium(I) Polypyridine Complexes with a Fluorous Pendant. *Organometallics* **2012**, *31*, 5844−5855.
(12) Gill, M. R.; Garcia-Lara, J.; Foster, S. J.; Smythe, C.; Battaglia, G.; Thomas, J. A. A Ruthenium(II) Polypyridyl Complex for Direct Imaging of DNA Structure in Living Cells. *Nat. Chem.* **2009**, *1*, 662−667.
(13) Ji, S.; Guo, H.; Wu, W.; Wu, W.; Zhao, J. Ruthenium(II) Polyimine−Coumarin Dyad with Non-Emissive ^{3}IL Excited State as Sensitizer for Triplet−Triplet Annihilation Based Upconversion. *Angew. Chem., Int. Ed.* **2011**, *50*, 8283−8286.
(14) Funaki, T.; Funakoshi, H.; Kitao, O.; Onozawa-Komatsuzaki, N.; Kasuga, K.; Sayama, K.; Sugihara, H. Cyclometalated Ruthenium-(II) Complexes as Near-IR Sensitizers for High Efficiency Dye-Sensitized Solar Cells. *Angew. Chem., Int. Ed.* **2012**, *51*, 7528−7531.
(15) Niu, Y.; Han, F.; Zhang, Q.; Xie, T.; Lu, L.; Li, S.; Xia, H. Off/On Fluorescent Chemosensors for Organotin Halides Based on Binuclear Ruthenium Complexes. *Angew. Chem., Int. Ed.* **2013**, *52*, 5599−5603.
(16) Gill, M. R.; Thomas, J. A. Ruthenium(II) Polypyridyl Complexes and DNA—from Structural Probes to Cellular Imaging and Therapeutics. *Chem. Soc. Rev.* **2012**, *41*, 3179−3192.
(17) Foxon, S. P.; Green, C.; Walker, M. G.; Wragg, A.; Adams, H.; Weinstein, J. A.; Parker, S. C.; Meijer, A. J.; Thomas, J. A. Synthesis, Characterization, and DNA Binding Properties of Ruthenium(II) Complexes Containing the Redox Active Ligand Benzo[*i*]dipyrido-[3,2-*a*:2′,3′-*c*]phenazine-11,16-quinone. *Inorg. Chem.* **2012**, *51*, 463−471.
(18) Baggaley, E.; Gill, M. R.; Green, N. H.; Turton, D.; Sazanovich, I. V.; Botchway, S. W.; Smythe, C.; Haycock, J. W.; Weinstein, J. A.; Thomas, J. A. Dinuclear Ruthenium(II) Complexes as Two-Photon, Time-Resolved Emission Microscopy Probes for Cellular DNA. *Angew. Chem., Int. Ed.* **2014**, *53*, 3367−3371.
(19) Xu, W. C.; Zuo, J. R.; Wang, L. L.; Ji, L. N. A.; Chao, H. Dinuclear Ruthenium(II) Polypyridyl Complexes as Single and Two-Photon Luminescence Cellular Imaging Probes. *Chem. Commun.* **2014**, *50*, 2123−2125.
(20) Steiner, M. S.; Duerkop, A. Luminescent Ruthenium Probe for the Determination of Acetyl Phosphate in Complex Biological Matrices. *Analyst* **2011**, *136*, 148−154.
(21) Zhang, R.; Ye, Z.; Yin, Y.; Wang, G.; Jin, D.; Yuan, J.; Piper, J. A. Developing Red-Emissive Ruthenium(II) Complex-Based Luminescent Probes for Cellular Imaging. *Bioconjugate Chem.* **2012**, *23*, 725−733.
(22) Chen, H.; Li, X.; Wu, Y.; Gao, W.; Bai, R. A Ruthenium(II) Complex with Environment-Responsive Dual Emission and Its Application in the Detection of Cysteine/Homocysteine. *Dalton Trans.* **2012**, *41*, 13292−13297.
(23) Zhang, R.; Ye, Z.; Song, B.; Dai, Z.; An, X.; Yuan, J. Development of a Ruthenium(II) Complex-Based Luminescent Probe for Hypochlorous Acid in Living Cells. *Inorg. Chem.* **2013**, *52*, 10325−10331.
(24) Zheng, Z. B.; Wu, Y. Q.; Wang, K. Z.; Li, F. pH Luminescence Switching, Dihydrogen Phosphate Sensing, and Cellular Uptake of a Heterobimetallic Ruthenium(II)−Rhenium(I) Complex. *Dalton Trans.* **2014**, *43*, 3273−3284.
(25) Chowdhury, B.; Khatua, S.; Dutta, R.; Chakraborty, S.; Ghosh, P. Bis-Heteroleptic Ruthenium(II) Complex of a Triazole Ligand as a Selective Probe for Phosphates. *Inorg. Chem.* **2014**, *53*, 8061−8070.
(26) Botchway, S. W.; Charnley, M.; Haycock, J. W.; Parker, A. W.; Rochester, D. L.; Weinstein, J. A.; Williams, J. A. G. Time-Resolved and Two-Photon Emission Imaging Microscopy of Live Cells with Inert Platinum Complexes. *Proc. Natl. Acad. Sci. U. S. A.* **2008**, *105*, 16071−16076.
(27) Jin, D. Y.; Piper, J. A. Time-Gated Luminescence Microscopy Allowing Direct Visual Inspection of Lanthanide-Stained Microorganisms in Background-Free Condition. *Anal. Chem.* **2011**, *83*, 2294−2300.
(28) Weitz, E. A.; Chang, J. Y.; Rosenfield, A. H.; Pierre, V. C. A Selective Luminescent Probe for the Direct Time-Gated Detection of Adenosine Triphosphate. *J. Am. Chem. Soc.* **2012**, *134*, 16099−16102.
(29) You, Y.; Lee, S.; Kim, T.; Ohkubo, K.; Chae, W. S.; Fukuzumi, S.; Jhon, G. J.; Nam, W.; Lippard, S. J. Phosphorescent Sensor for Biological Mobile Zinc. *J. Am. Chem. Soc.* **2011**, *133*, 18328−18342.
(30) Huang, K.; Marti, A. A. Optimizing the Sensitivity of Photoluminescent Probes Using Time-Resolved Spectroscopy: A Molecular Beacon Case Study. *Anal. Chem.* **2012**, *84*, 8075−8082.
(31) Shi, H. F.; Sun, H. B.; Yang, H. R.; Liu, S. J.; Jenkins, G.; Feng, W.; Li, F. Y.; Zhao, Q.; Liu, B.; Huang, W. Cationic Polyfluorenes with Phosphorescent Iridium(III) Complexes for Time-Resolved Luminescent Biosensing and Fluorescence Lifetime Imaging. *Adv. Funct. Mater.* **2013**, *23*, 3268−3276.
(32) Tang, Y.; Yang, H.; Sun, H.; Liu, S.; Wang, J.; Zhao, Q.; Liu, X.; Xu, W.; Li, S.; Huang, W. Rational Design of an "OFF−ON" Phosphorescent Chemodosimeter Based on an Iridium(III) Complex and Its Application for Time-Resolved Luminescent Detection and Bioimaging of Cysteine and Homocysteine. *Chem.—Eur. J.* **2013**, *19*, 1311−1319.
(33) Xu, W.; Zhao, X.; Lv, W.; Yang, H.; Liu, S.; Liang, H.; Tu, Z.; Xu, H.; Qiao, W.; Zhao, Q.; Huang, W. Rational Design of Phosphorescent Chemodosimeter for Reaction-Based One- and Two-Photon and Time-Resolved Luminescent Imaging of Biothiols in Living Cells. *Adv. Healthcare Mater.* **2014**, *3*, 658−669.
(34) Hanaoka, K.; Kikuchi, K.; Kobayashi, S.; Nagano, T. Time-Resolved Long-Lived Luminescence Imaging Method Employing Luminescent Lanthanide Probes with a New Microscopy System. *J. Am. Chem. Soc.* **2007**, *129*, 13502−13509.
(35) Zhang, L.; Tian, L.; Ye, Z.; Song, B.; Yuan, J. Preparation of Visible-Light-Excited Europium Biolabels for Time-Resolved Luminescence Cell Imaging Application. *Talanta* **2013**, *108*, 143−149.
(36) McMahon, B. K.; Gunnlaugsson, T. Lanthanide Luminescence Sensing of Copper and Mercury Ions Using an Iminodiacetate-Based Tb(III)-Cyclen Chemosensor. *Tetrahedron Lett.* **2010**, *51*, 5406−5410.
(37) Tan, H. L.; Zhang, Y. Q.; Chen, Y. Detection of Mercury Ions (Hg2+) in Urine Using a Terbium Chelate Fluorescent Probe. *Sens. Actuators, B* **2011**, *156*, 120−125.
(38) Cui, G. F.; Ye, Z. Q.; Zhang, R.; Wang, G. L.; Yuan, J. L. Design and Synthesis of a Terbium(III) Complex-Based Luminescence Probe for Time-Gated Luminescence Detection of Mercury(II) Ions. *J. Fluoresc.* **2012**, *22*, 261−267.
(39) McMahon, B. K.; Pal, R.; Parker, D. A Bright and Responsive Europium Probe for Determination of pH Change within the Endoplasmic Reticulum of Living Cells. *Chem. Commun.* **2013**, *49*, 5363−5365.
(40) Duong, T. Q.; Kim, J. S. Fluoro- and Chromogenic Chemodosimeters for Heavy Metal Ion Detection in Solution and Biospecimens. *Chem. Rev.* **2010**, *110*, 6280−6301.
(41) Chen, X.; Pradhan, T.; Wang, F.; Kim, J. S.; Yoon, J. Fluorescent Chemosensors Based on Spiroring-Opening of Xanthenes and Related Derivatives. *Chem. Rev.* **2012**, *112*, 1910−1956.
(42) Yang, Y.; Zhao, Q.; Feng, W.; Li, F. Luminescent Chemodosimeters for Bioimaging. *Chem. Rev.* **2013**, *113*, 192−270.
(43) Carter, K. P.; Young, A. M.; Palmer, A. E. Fluorescent Sensors for Measuring Metal Ions in Living Systems. *Chem. Rev.* **2014**, *114*, 4564−4601.
(44) Srivastava, P.; Razi, S. S.; Ali, R.; Gupta, R. C.; Yadav, S. S.; Narayan, G.; Misra, A. Selective Naked-Eye Detection of Hg^{2+} through an Efficient Turn-On Photoinduced Electron Transfer Fluorescent Probe and Its Real Applications. *Anal. Chem.* **2014**, *86*, 8693−8699.

DOI: 10.1021/am508484q
ACS Appl. Mater. Interfaces 2015, 7, 4247−4256

(45) Srivastava, P.; Ali, R.; Razi, S. S.; Shahid, M.; Patnaik, S.; Misra, A. A Simple Blue Fluorescent Probe to Detect Hg^{2+} in Semiaqueous Environment by Intramolecular Charge Transfer Mechanism. *Tetrahedron Lett.* **2013**, *54*, 3688−3693.
(46) Tchounwou, P. B.; Ayensu, W. K.; Ninashvili, N.; Sutton, D. Environmental Exposure to Mercury and Its Toxicopathologic Implications for Public Health. *Environ. Toxicol.* **2003**, *18*, 149−175.
(47) Lee, R.; Middleton, D.; Caldwell, K.; Dearwent, S.; Jones, S.; Lewis, B.; Monteilh, C.; Mortensen, M. E.; Nickle, R.; Orloff, K.; Reger, M.; Risher, J.; Rogers, H. S.; Watters, M. A Review of Events That Expose Children to Elemental Mercury in the United States. *Environ. Health Perspect.* **2009**, *117*, 871−878.
(48) Tong, Y.; Zhang, W.; Chen, C.; Chen, L.; Wang, W.; Hu, X.; Wang, H.; Hu, D.; Ou, L.; Wang, X.; Wang, Q. Fate Modeling of Mercury Species and Fluxes Estimation in an Urban River. *Environ. Pollut.* **2014**, *184*, 54−61.
(49) Nolan, E. M.; Lippard, S. J. Tools and Tactics for the Optical Detection of Mercuric Ion. *Chem. Rev.* **2008**, *108*, 3443−3480.
(50) Liu, B.; Tian, H. A Selective Fluorescent Ratiometric Chemodosimeter for Mercury Ion. *Chem. Commun.* **2005**, 3156−3158.
(51) Wu, J.; Hwang, I.; Kim, K. S.; Kim, J. S. Rhodamine-Based Hg^{2+}-Selective Chemodosimeter in Aqueous Solution: Fluorescent OFF−ON. *Org. Lett.* **2007**, *9*, 907−910.
(52) Srivastava, P.; Ali, R.; Razi, S. S.; Shahid, M.; Misra, A. Thiourea Based Molecular Dyad (ANTU): Fluorogenic Hg^{2+} Selective Chemodosimeter Exhibiting Blue−Green Fluorescence in Aqueous-Ethanol Environment. *Sens. Actuators, B* **2013**, *181*, 584−595.
(53) Nakamura, K. Synthesis, Luminescence Quantum Yields, and Lifetimes of Trischelated Ruthenium(II) Mixed-Ligand Complexes Including 3,3′-Dimethyl-2,2′-Bipyridyl. *Bull. Chem. Soc. Jpn.* **1982**, *55*, 2697−2705.
(54) Frisch, M. J.; Trucks, G. W.; Schlegel, H. B.; Scuseria, G. E.; Robb, M. A.; Cheeseman, J. R.; Scalmani, G.; Barone, V.; Mennucci, B.; Petersson, G. A.; Nakatsuji, H.; Caricato, M.; Li, X.; Hratchian, H. P.; Izmaylov, A. F.; Bloino, J.; Zheng, G.; Sonnenberg, J. L.; Hada, M.; Ehara, M.; Toyota, K.; Fukuda, R.; Hasegawa, J.; Ishida, M.; Nakajima, T.; Honda, Y.; Kitao, O.; Nakai, H.; Vreven, T.; Montgomery, J. A., Jr.; Peralta, J. E.; Ogliaro, F.; Bearpark, M.; Heyd, J. J.; Brothers, E.; Kudin, K. N.; Staroverov, V. N.; Kobayashi, R.; Normand, J.; Raghavachari, K.; Rendell, A.; Burant, J. C.; Iyengar, S. S.; Tomasi, J.; Cossi, M.; Rega, N.; Millam, N. J.; Klene, M.; Knox, J. E.; Cross, J. B.; Bakken, V.; Adamo, C.; Jaramillo, J.; Gomperts, R.; Stratmann, R. E.; Yazyev, O.; Austin, A. J.; Cammi, R.; Pomelli, C.; Ochterski, J. W.; Martin, R. L.; Morokuma, K.; Zakrzewski, V. G.; Voth, G. A.; Salvador, P.; Dannenberg, J. J.; Dapprich, S.; Daniels, A. D.; Farkas, O.; Foresman, J. B.; Ortiz, J. V.; Cioslowski, J.; Fox, D. J. *Gaussian 09*, Revision A.01; Gaussian, Inc.: Wallingford, CT, 2009.
(55) Lee, C.; Yang, W.; Parr, R. G. Development of the Colle-Salvetti Correlation-Energy Formula into a Functional of the Electron Density. *Phys. Rev. B* **1988**, *37*, 785−789.
(56) Hay, P. J.; Wadt, W. R. Ab Initio Effective Core Potentials for Molecular Calculations. Potentials for the Transition Metal Atoms Sc to Hg. *J. Chem. Phys.* **1985**, *82*, 270−283.
(57) Hehre, W. J.; Ditchfield, R.; Pople, J. A. Self-Consistent Molecular Orbital Methods. XII. Further Extensions of Gaussian—Type Basis Sets for Use in Molecular Orbital Studies of Organic Molecules. *J. Chem. Phys.* **1972**, *56*, 2257−2261.
(58) Stratmann, R. E.; Scuseria, G. E.; Frisch, M. J. An Efficient Implementation of Time-Dependent Density-Functional Theory for the Calculation of Excitation Energies of Large Molecules. *J. Chem. Phys.* **1998**, *109*, 8218−8224.
(59) Cossi, M.; Barone, V. Time-Dependent Density Functional Theory for Molecules in Liquid Solutions. *J. Chem. Phys.* **2001**, *115*, 4708−4717.
(60) Lu, T.; Chen, F. Calculation of Molecular Orbital Composition. *Acta Chim. Sin.* **2011**, *69*, 2393−2406.
(61) Boens, N.; Qin, W.; Basarić, N.; Hofkens, J.; Ameloot, M.; Pouget, J.; Lefevre, J. P.; Valeur, B.; Gratton, E.; vandeVen, M.; Silva, N. D., Jr.; Engelborghs, Y.; Willaert, K.; Sillen, A.; Rumbles, G.; Phillips, D.; Visser, A. J.; van Hoek, A.; Lakowicz, J. R.; Malak, H.; Gryczynski, I.; Szabo, A. G.; Krajcarski, D. T.; Tamai, N.; Miura, A. Fluorescence Lifetime Standards for Time and Frequency Domain Fluorescence Spectroscopy. *Anal. Chem.* **2007**, *79*, 2137−2149.
(62) Mosmann, T. J. Rapid Colorimetric Assay for Cellular Growth and Survival: Application to Proliferation and Cytotoxicity Assays. *Immunol. Methods* **1983**, *65*, 55−63.
(63) *Mercury Update: Impact on Fish Advisories. EPA Fact Sheet EPA-823-F-01-011;* EPA, Office of Water: Washington, DC, 2001.

NOTE ADDED AFTER ASAP PUBLICATION

This paper was published on the Web on February 10, 2015, with the graphics for Figures 6 and 7 reversed. The corrected version was reposted on February 12, 2015.

DOI: 10.1021/am508484q
ACS Appl. Mater. Interfaces 2015, 7, 4247−4256